

Article

Investigation of Multiple High Quality-Factor Fano Resonances in Asymmetric Nanopillar Arrays for Optical Sensing

Huawei Chen ¹, Xinye Fan ^{1,2,3,4,*}, Wenjing Fang ^{1,3,4}, Shuangshuang Cao ¹, Qinghe Sun ¹, Dandan Wang ¹, Huijuan Niu ^{1,3,4}, Chuanchuan Li ², Xin Wei ², Chenglin Bai ^{1,3,4}  and Santosh Kumar ^{5,*} 

¹ School of Physics Science and Information Engineering, Liaocheng University, Liaocheng 252000, China

² Institute of Semiconductors, Chinese Academy of Sciences, Beijing 100083, China

³ Shandong Provincial Key Laboratory of Optical Communication Science and Technology, Liaocheng 252000, China

⁴ Liaocheng Key Laboratory of Industrial-Internet Research and Application, Liaocheng 252000, China

⁵ Department of Electronics and Communication Engineering, K L Deemed to be University, Guntur 522302, India

* Correspondence: fanxinye@lcu.edu.cn (X.F.); santosh@kluniversity.in (S.K.)

Abstract: A novel asymmetric all-dielectric metasurface supporting multiple Fano resonances with high quality-factor through the excitation of quasi-bound states in the continuum is theoretically investigated. It is demonstrated that two resonances in the near-infrared wavelength are excited by the symmetry-protected bound state in the continuum, which can be transformed into the electric dipole and the toroidal dipole quasi-BIC resonance with high quality-factor by breaking the symmetry of metasurface. Moreover, the sensing properties based on different liquid refractive indexes are researched theoretically. The results show that the maximum quality-factor of the Fano resonance peak is 8422, and the sensitivity can reach 402 nm/RIU, with a maximum figure of merit of 2400 RIU⁻¹. This research is believed to further promote the development of optical sensing and nonlinear optics.

Keywords: all-dielectric; high Q-factor; metasurface



Citation: Chen, H.; Fan, X.; Fang, W.; Cao, S.; Sun, Q.; Wang, D.; Niu, H.; Li, C.; Wei, X.; Bai, C.; et al. Investigation of Multiple High Quality-Factor Fano Resonances in Asymmetric Nanopillar Arrays for Optical Sensing. *Photonics* **2024**, *11*, 68. <https://doi.org/10.3390/photonics11010068>

Received: 3 November 2023

Revised: 3 January 2024

Accepted: 5 January 2024

Published: 8 January 2024



Copyright: © 2024 by the authors. Licensee MDPI, Basel, Switzerland. This article is an open access article distributed under the terms and conditions of the Creative Commons Attribution (CC BY) license (<https://creativecommons.org/licenses/by/4.0/>).

1. Introduction

As a two-dimensional metamaterial, metasurfaces can be artificially engineered into subwavelength structures to obtain electromagnetic properties not found in natural materials [1,2]. By optimizing the structural parameters of the metasurface, high quality-factor (Q-factor) Fano resonances are achieved, which have important roles in the fields of optical refractive index sensing [3,4], optical switches [5], nonlinear optics [6,7], and slow light [8]. The high Q-factor Fano resonance not only enhances the light-matter interactions but also has a high sensitivity to tiny environmental changes [9,10].

High Q-factor Fano resonances are obtained in many ways. Mohammadi et al. presented a photonic crystal ring resonator including three different photonic crystal sensors with Q-factors up to 5365 [11]. Zhou et al. designed a guided-mode resonance sensor with a shallow subwavelength structure with a Q-factor up to 8000 [12]. All-dielectric metasurfaces offer greater freedom and design flexibility, allowing for more diversified functionality [13]. Different optical functions can be achieved by precisely designing nanostructures that allow precise modulation of several parameters of light, such as polarization, wavelength, phase, and amplitude [14]. At the same time, the all-dielectric metasurface is capable of wide-bandwidth functionality, allowing simultaneous operation of resonances in multiple frequency ranges. In addition, all-dielectric metasurface sensors have better tunability. Wavelength selectivity of the sensor is achieved by adjusting the geometry of the structure, material properties or electromagnetic excitation.

In recent years, silicon nitride has been an important member of the silicon-based family for making resonators [15,16]. Yang et al. designed a refractive index sensor based

on bilayer silicon nitride with a Q-factor of 7605 [17]. Guo et al. proposed an all-dielectric metasurface based on a silicon nitride substrate, where the Q-factor of the resonance peak can reach 54757 [18]. In addition, silicon nitride is widely used in a variety of resonators (drum resonators [19], micro-ring resonators [20], waveguide-coupled resonators [21,22]), oscillators [23], and semiconductor lasers [24]). Silicon nitride-based optics can reach Q-factors of the order of 10^6 in most cases, with the highest reaching 2.6×10^8 . Although silicon nitride resonators have extremely high Q-factors, all-dielectric metasurface sensors composed of silicon and silicon dioxide are still very necessary because silicon and silicon dioxide are easily manufactured using current manufacturing techniques [25]. The all-dielectric metasurface composed of silicon and silica can excite multiple Fano resonance peaks simultaneously. More resonant peaks are better suited for multi-channel sensing applications [26].

The all-dielectric metasurface is believed to be a great way to obtain high Q-factor Fano resonance due to its greater freedom, design flexibility, and compatibility with complementary metal oxide semiconductor (CMOS) processes [27]. The excitation of Fano resonance in metasurfaces has evolved from a single resonance peak to multiple resonance peaks with the development of sensing technology [28,29]. Multi-Fano resonances have potential applications in the fields of multi-wavelength sensing and multi-channel biosensing [30]. Yang et al. proposed an all-dielectric metasurfaces consisting of an array of square nanopores, which excited four Fano resonances by introducing nanopore asymmetry [31]. Wang et al. investigated an all-dielectric metasurface consisting of an asymmetric nanocylindrical dimer with five Fano resonance peaks that were excited [28].

An efficient way for generating high Q-factor Fano resonances in all-dielectric metasurfaces is through the utilization of bound states in the continuum (BIC) [32,33]. The BIC is a non-radiative state characterized by a resonance frequency embedded in the continuum spectrum of radiative modes in the surrounding space. The coupling of the resonant mode to the surrounding external channels is prohibited when symmetry is maintained, and this type of BIC is referred to as a symmetry-protected BIC [34,35], which is considered to be an ideal BIC arising from an infinitely high Q-factor and extremely narrow resonance width [36,37]. However, this ideal BIC cannot be observed because of the absence of far-field radiation and the inability to be excited by incident waves. It is necessary to create a radiation channel to the outside by breaking the symmetry of the result or by oblique incidence of the light source [38]. Through this method, the symmetry-protected BIC is switched to the quasi-BIC mode so that the Q-factor of the resonance becomes finite [39,40].

In this paper, an all-dielectric metasurface that can excite multiple Fano resonance peaks in the near-infrared spectral region is designed and simulated. The metasurface is consisting of five rectangular silicon blocks periodically placed on a silica-based substrate. Changing the length of two of the rectangular silicon blocks breaks the symmetry of the structure, and thus, four Fano resonance peaks are excited. The Q-factors of the four Fano resonance peaks all reach 10^3 , and the highest can reach 8422, the sensitivity is up to 402 nm/RIU, and the figure of merit (FOM) can reach up to 2400 RIU^{-1} . The preparation process of the structure is investigated as a way to demonstrate the realizability of the structure. It is shown that the structure has potential applications in the field of refractive index sensors.

2. Structure Design

The schematics of the designed metasurface structure are shown in Figure 1. Figure 1a shows the array layout of the structure, which is periodically distributed on a substrate with the material SiO_2 . The structure of a single cell is shown in Figure 1b, where the labeled P_x and P_y denote the period in the x and y directions, respectively, and h is the height of the silicon block. Figure 1c shows the top view of the structure, the length of the two rectangular blocks on the left (L_1) is 280 nm, the length of the two rectangular blocks on the right (L_2) is 170 nm, the length of the rectangular blocks in the center (L_3) is 660 nm, the width of the rectangular blocks (w) is 150 nm, and the distance between

the rectangular blocks (g) is 100 nm. The structure is asymmetrical along the y -axis since $L_1 \neq L_2$. $\delta = L_1 - L_2$ as an asymmetry parameter is used to explore the effect of asymmetry on the excitation of the Fano resonance peaks.

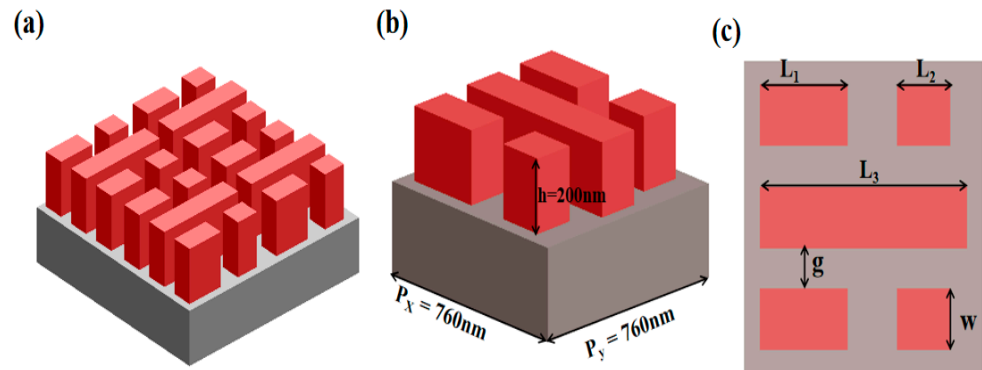


Figure 1. Schematic of the metasurface structure consisting of five rectangular columns. (a) Structural layout of the designed metasurface; (b) diagram of the structure of a single cell; (c) top view of a single cell.

The system of Maxwell’s equations is transformed into finite difference equations by the finite difference in time domain (FDTD) method, enabling the simulations to be conducted. With this method, the distribution information of the electromagnetic field can be calculated when the boundary conditions and initial values are known, which greatly reduces the difficulty of the calculation. In the simulation, it is necessary to set the appropriate mesh size. The resolution of the mesh needs to be detailed enough to capture the details and rapidly changing features that appear in the simulation. Excessive mesh size leads to a decrease in the accuracy of the simulation results, as tiny structures and details cannot be adequately represented. If the mesh size is too small, it will lead to an increase in the computational effort, thus decreasing the computational efficiency. Therefore, the mesh was set to $8 \text{ nm} \times 8 \text{ nm} \times 8 \text{ nm}$ during the simulation. In order to simulate the behavior of a system in three dimensions, boundary conditions need to be set. In this case, the X and Y directions are set to periodic boundary conditions, which means the simulation accurately represents the behavior of the system across multiple repetitions. On the other hand, the Z direction is set to Perfectly Matched Layer (PML). This is a type of boundary condition that effectively absorbs outgoing waves in the system, preventing reflections and ensuring accurate results. By combining periodic boundary conditions in the X and Y directions with a PML boundary condition in the Z direction, a comprehensive and reliable simulation can be achieved. The y -polarized plane wave perpendicular to the z -axis as a light source is used in the simulations. The plane wave is used in the simulation process. Plane waves propagate through space at a constant velocity without changing shape or decaying. Optical parameters of silicon and silicon dioxide used in the simulations are referenced in the Palik manual.

3. Results and Discussion

The transmission spectrum of the structure in the liquid refractive index of 1.35 state is simulated, while the background refractive index is set to $n = 1.35$. When $L_1 = L_2$ ($\delta = 0 \text{ nm}$), the transmission spectrum is obtained as shown by the black solid line in Figure 2a. Two Fano resonance peaks marked as R1 and R2 are observed at the wavelength of 1123 nm and 1163 nm, respectively. The asymmetric metasurface transmission spectrum is shown in Figure 2b. Two new Fano resonance peaks, labeled R3 and R4, are innovatively excited at 1202 nm and 1221 nm when the length of L_2 is changed to 170 nm ($\delta = 110 \text{ nm}$). As the symmetry of the metasurface is broken, radiation channels are established, allowing energy to leak outward, resulting in a symmetry-protected BIC converting to a quasi-BIC.

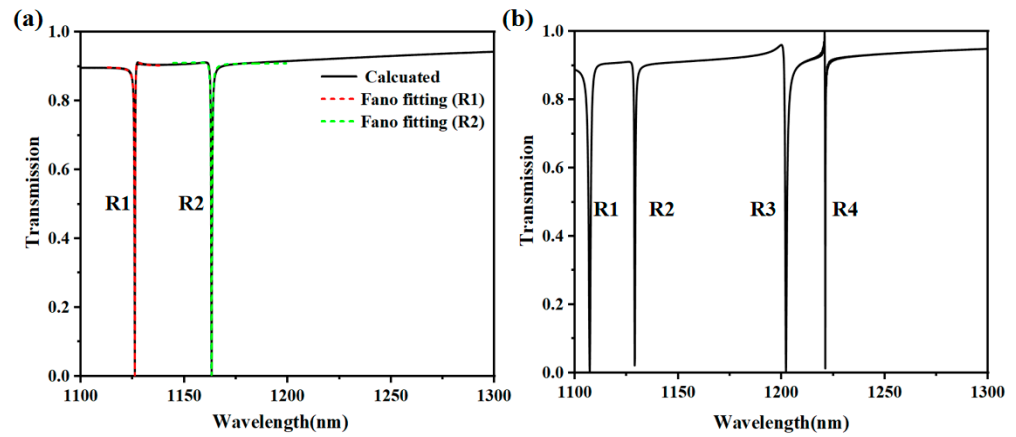


Figure 2. Simulated transmission spectra of the metasurface. (a) Transmission spectrum of symmetric structure and equation fitting plot; (b) transmission spectrum of asymmetric structure.

In addition, the excited Fano resonance peaks of the periodic all-dielectric metasurface can be analyzed and fitted by the Fano model with Equation (1) [36]:

$$T = \left| a_1 + ia_2 + \frac{b}{\omega - \omega_0 + i\gamma} \right|^2 \quad (1)$$

where a_1 , a_2 , and b are constant real numbers, ω_0 is the resonant frequency, and γ is the damping loss. The Fano curves fitted by Equation (1) are shown as red and green dashed lines in Figure 2a. The fitting results are in general agreement with the simulation results. Equation (2) is extracted by Equation (1), and the Q-factor of the Fano resonance can be obtained by Equation (2).

$$Q = \frac{\omega_0}{2\gamma} \quad (2)$$

The Q-factors of the Fano resonance peaks are calculated when $\delta = 110$ nm: 1054 ($\omega_0 = 1.122$ eV and $\gamma = 0.5323 \times 10^{-3}$ eV), 2377 ($\omega_0 = 1.101$ eV and $\gamma = 0.2316 \times 10^{-3}$ eV), 1336 ($\omega_0 = 1.336$ eV and $\gamma = 0.3868 \times 10^{-3}$ eV), 8422 ($\omega_0 = 1.0174$ eV and $\gamma = 0.0604 \times 10^{-3}$ eV).

The relationship between the Q-factor and the degree of asymmetry is discussed. $\alpha = \Delta S/S$ as the degree of asymmetry, where S is the area of the silicon block when symmetric and ΔS is the area of the reduced silicon block when asymmetric. As ΔS decreases, the Q-factor is larger. After observing several sets of data, the Q-factor of the excited Fano resonance is found to be related to the degree of asymmetry as $Q \propto \alpha^{-2}$, as shown in Figure 3a.

In order to further investigate the nature of the multiple resonance peaks generated by this metasurface, the electromagnetic field distributions of the resonance peaks under asymmetry are simulated, and their near-field distribution is shown in Figure 4. For the resonance peak R1, the magnetic field forms two clockwise loops in the x-z plane, and the electric field is linear in the x-y plane, which is a typical electric dipole (ED) feature. The resonance mode of R3 is also considered to be ED, but its direction is opposite to that of R1. The resonance mode of R2 can be seen in the figure as magnetic dipoles (MDs), in which the current forms three loops with the same direction in the y-z plane and the magnetic field is linearly polarized in the x-y plane. Two current loops in opposite directions can be observed in the x-y plane of R4, and the resulting magnetic field creates a large loop in the x-z plane, which is typical of toroidal dipole (TD) resonance.

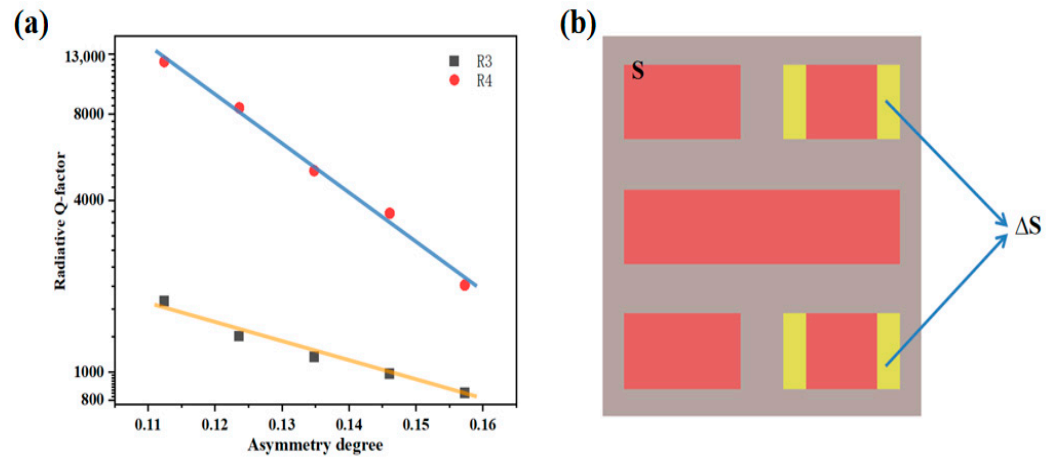


Figure 3. (a) Plot of the Q-factor of the excited Fano resonance versus the degree of asymmetry α ; (b) schematic representation of ΔS and S .

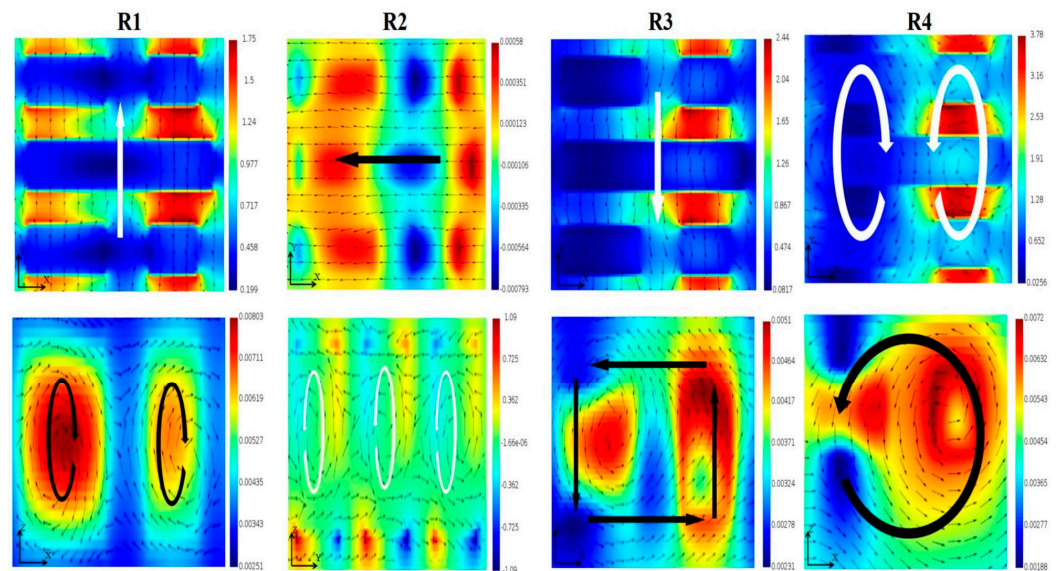


Figure 4. Near-field distribution of the electromagnetic field corresponding to the four Fano resonance peaks in the asymmetric case. The electric field vector distributions are shown as white arrows and the magnetic field vector distributions are shown as black arrows.

The characteristics of the transmission spectrum for different geometrical parameters are also discussed to obtain the optimal parameter, and the simulation results are shown in Figure 5. Figure 5a shows the transmission spectrums of the silicon block with a high between 180 nm and 220 nm, and it is clear that the resonance peaks are sensitive because the four resonance peaks red-shift as h increases, especially R1. The transmission spectrums of the silicon block with a wide w between 130 nm and 170 nm are presented in Figure 5b, where all the four resonance peaks are red-shifted with w increasing. In addition, the linewidth of R1 decreases as w increases, and the modulation depth of R4 becomes deeper as w increases. The transmission spectrum corresponding to the change in length of the intermediate silicon block (L_3) is displayed in Figure 5c. The L_3 produces little effect on the transmission spectrum of the metasurface. Figure 5d parades the transmission spectra at different periods. The Fano resonance peaks show different degrees of red-shift as the period increases. However, compared with h and w , this red-shift is slight, while the modulation depth of R4 undergoes a little change.

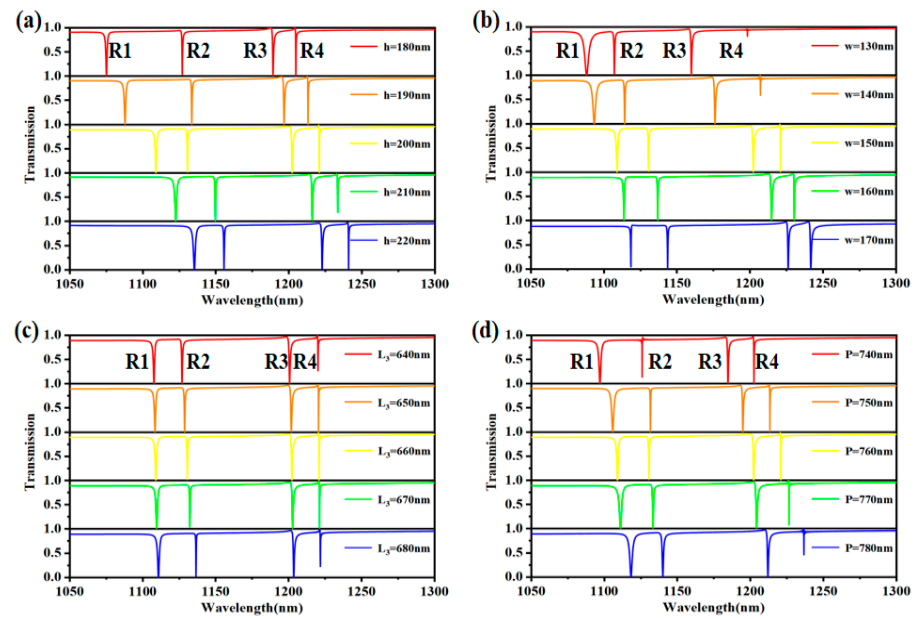


Figure 5. Transmission spectra of the metasurface with varying geometrical parameters. (a) Height of the silicon block (h), (b) width of the silicon block (w), (c) length of the middle silicon block (L_3), and (d) period of the metasurface (P).

In order to investigate the influence of light absorption and scattering caused by liquid and materials on the transmission spectrum of the structure, different extinction coefficients (k) are set for symmetric and asymmetric cases, respectively. The simulation results are shown in Figure 6. The linewidth of the resonance peak increases with increasing extinction coefficient; however, the modulation depth and Q-factor decrease. The sensitivity of the resonance peaks to the extinction coefficient varies, with R4 being the most sensitive and R1 the least sensitive. What this result presents is that the same extinction coefficient will have different effects on the Fano resonance formed by different resonant modes. These simulations demonstrated that the presence of a large intrinsic absorption in the liquid and materials used would cause the resonance to attenuate or even disappear.

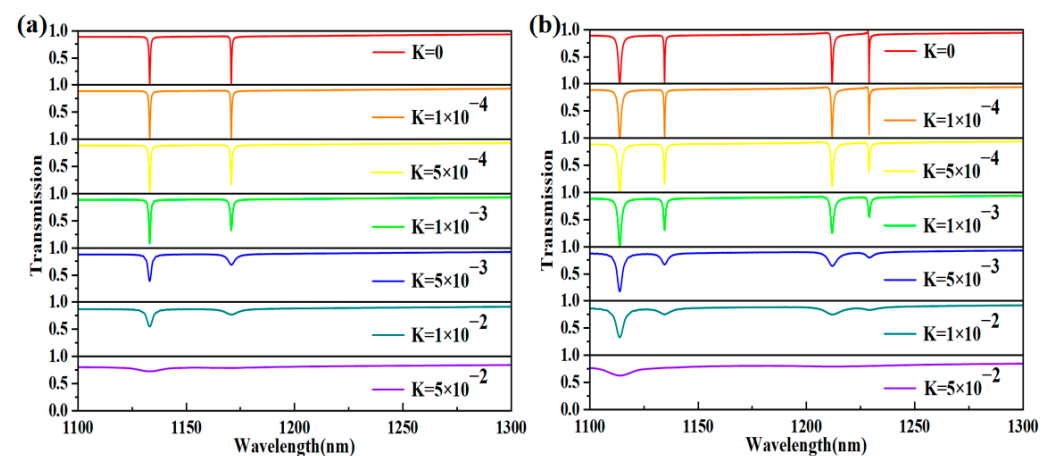


Figure 6. (a) Transmission spectra of symmetric structures with different extinction coefficients, (b) Transmission spectra of asymmetric structures with different extinction coefficients.

The proposed metastructure is shown to be investigated as a refractive index sensor due to its advantages of excitation of high Q-factor Fano resonance and local field enhancement. The potential application of metasurfaces in the field of refractive index sensors is verified by analyzing the changing patterns of transmission spectra at different

ambient refractive indexes. Figure 7 show the transmission spectra of R1, R2, R3, and R4 at ambient refractive index (n) in steps of 0.01 from 1.33 to 1.37, respectively. As can be seen from Figure 7, the Fano resonance peaks are significantly red-shifted despite the little change in refractive index. The sensing performance of the metasurface is believed to be determined by two metrics, the sensitivity S and the FOM. The sensitivity is calculated by Equation (3) [41]:

$$S = \frac{\Delta\lambda(\text{nm})}{\Delta n(\text{RIU})} \tag{3}$$

in which $\Delta\lambda$ is the offset of the resonance peak and Δn is the difference in refractive index. Refractive index unit (RIU) represents the ratio of the speed of light relative to the speed of light in a vacuum as it enters the medium from a vacuum. The sensitivities of the Fano resonance peaks are 129, 333, 403, 348 by calculation. Figure 7b,d show the wavelengths corresponding to the four resonance peaks at different refractive indexes, and the slope of the curve corresponding to each resonance peak is the sensitivity of that resonance peak. The FOM is calculated by Equation (4) [42]:

$$\text{FOM} = \frac{S(\text{nm/RIU})}{\text{FWHM}(\text{nm})} \tag{4}$$

in which S is the sensitivity and FWHM is the full width at half peak of the resonance peak. The FOM corresponding to the four resonance peaks is calculated to be 123, 701, 448, and 2400, respectively.

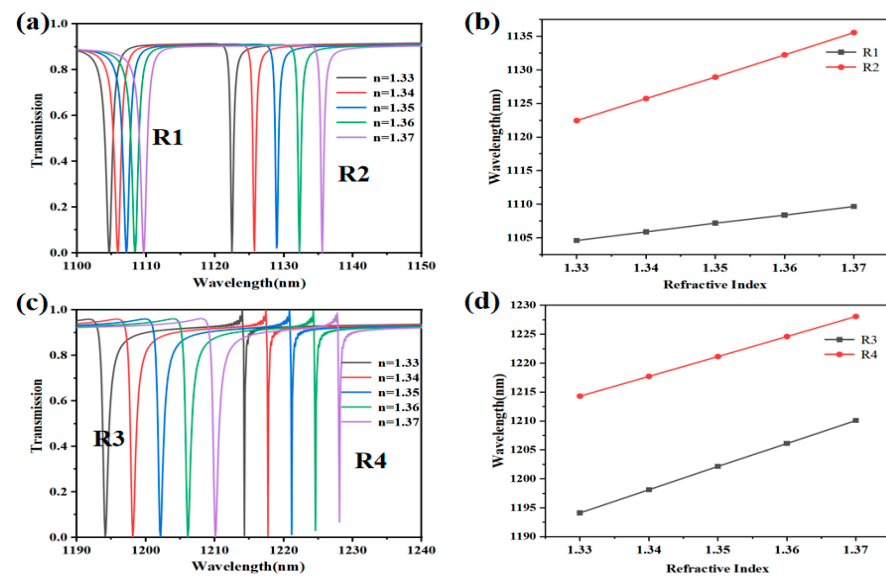


Figure 7. Transmission spectra of metasurfaces at different refractive indexes. (a) Transmission spectra of R1 and R2 at different refractive indexes; (b) wavelength plots corresponding to R1 and R2 at different refractive indexes; (c) transmission spectra of R3 and R4 at different refractive indexes; (d) wavelength plots corresponding to R3 and R4 at different refractive indexes.

In addition, the proposed metastructure is compared with the existing work for number of resonance peaks, sensitivity, and FOM, as shown in Table 1. The results show that the metastructure proposed in this paper can generate more resonance peaks with higher sensitivity and FOM, which is more suitable for multichannel sensing applications.

Table 1. The number of resonance peaks, sensitivity, and FOM of this sensor are compared with other types.

Sensor Type	Number of Resonance Peaks	S (nm/RIU)	FOM (RIU ⁻¹)	Ref.
Double square hollow	4	287.5	389	[29]
U-shaped silicon cylinder	1	203	29	[43]
Split-ring disk	2	282	4	[44]
Optical sensor based on a photonic crystal metasurface	2	178	445	[45]
Bilayer Silicon Nitride Photonic Crystal Sensor	1	937.64	n.r. ^a	[17]
All-dielectric metasurface based on a silicon nitride substrate	2	746	18650	[18]
Five rectangular blocks of silicon	4	403	2400	This work

^a not reported.

The proposed sensors are mainly based on silicon on insulator (SOI) fabrication. SOI device processes are compatible with standard silicon CMOS processes, which are easy and inexpensive to fabricate, making them ideal for large-scale semiconductor chip integration. The preparation process of the proposed metastructure is shown in Figure 8. The device preparation procedure consists of the following steps: cleaning of the SOI substrate, low-pressure chemical vapor deposition (LPCVD), spin coating of the resist, electron beam lithography (EBL), development, inductively coupled plasma (ICP) etching and removal of the resist.

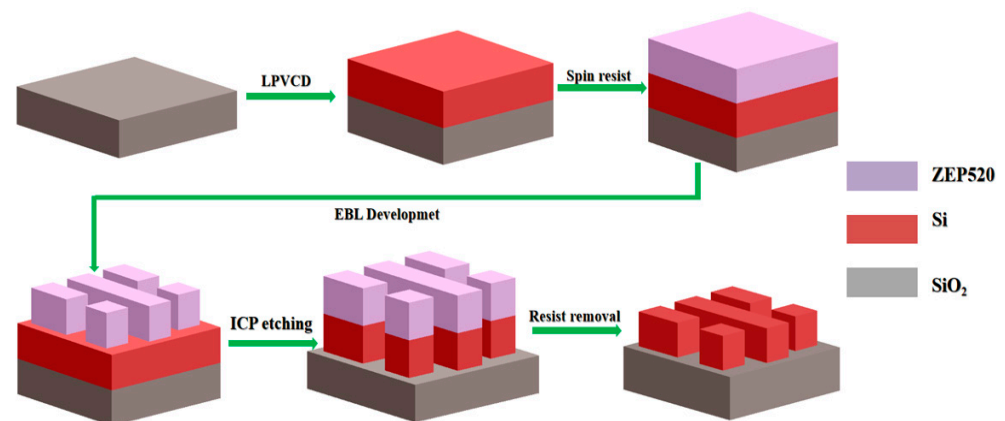


Figure 8. The fabrication process flow chart of the metastructure.

4. Conclusions

In summary, we proposed and theoretically demonstrated a structure-asymmetric all-dielectric metasurface based on asymmetric nanopillar arrays. Four sharp and high-spectral-contrast Fano resonances are excited with the best Q-factor of 8422. The results of the electromagnetic field distribution explicate that the resonances at 1107 nm and 1202 nm are governed by the ED mode, while the resonances at 1129 nm and 1221 nm are governed by the MDs mode and TD mode, respectively. In addition, the relationship between the different extinction coefficients (K) and transmission spectrum indicates that the resonances are attenuated or even disappear, occurring when there is a large intrinsic absorption in the liquid. Finally, the sensing characteristics based on different liquid refractive indices are analyzed to certify that the designed all-dielectric metasurface is employed as a refractive index sensor with the maximum sensitivity, and the FOM value is

402 nm/RIU and 2400 RIU⁻¹, respectively. This dielectric metasurface with multiple sharp resonances offers a good platform for multichannel sensing as well as optical modulation.

Author Contributions: Writing—original draft preparation, H.C.; writing—review and editing, X.F., W.F., S.C., Q.S., D.W., C.L., X.W. and S.K.; project administration, funding acquisition—X.F., W.F., H.N., C.B. and S.K. All authors have read and agreed to the published version of the manuscript.

Funding: This work is supported by the Cultivation Plan for Young Scholars in Universities of Shandong Province (2021RC085); The Natural Foundation of Shandong Province (ZR2021MF053, ZR2022MF253, ZR2021MF070, and ZR2022MF305); The Open Fund of the Key State Laboratory (BUPT, IPOC) (IPOC2021B07); The Double-Hundred Talent Plan of Shandong Province, China; Liaocheng University (318052341).

Institutional Review Board Statement: Not applicable.

Informed Consent Statement: Not applicable.

Data Availability Statement: The data supporting the findings of this study are available from the corresponding authors upon reasonable request.

Conflicts of Interest: The authors declare no conflict of interest.

References

- Zhang, F.; Pu, M.; Gao, P.; Jin, J.; Li, X.; Guo, Y.; Ma, X.; Luo, J.; Hong, Y.; Luo, X. Simultaneous Full-Color Printing and Holography Enabled by Centimeter-Scale Plasmonic Metasurfaces. *Adv. Sci.* **2020**, *7*, 1903156. [[CrossRef](#)]
- Alhalaby, H.; Principe, M.; Zaraket, H.; Vaiano, P.; Aliberti, A.; Quero, G.; Crescitelli, A.; Di Meo, V.; Esposito, E.; Consales, M.; et al. Design and Optimization of All-Dielectric Fluorescence Enhancing Metasurfaces: Towards Advanced Metasurface-Assisted Optodes. *Biosensors* **2022**, *12*, 264. [[CrossRef](#)] [[PubMed](#)]
- Zhang, Y.; Liu, W.; Li, Z.; Li, Z.; Cheng, H.; Chen, S.; Tian, J. High-quality-factor multiple Fano resonances for refractive index sensing. *Opt. Lett.* **2018**, *43*, 1842–1845. [[CrossRef](#)] [[PubMed](#)]
- Song, S.; Yu, S.; Li, H.; Zhao, T. Ultra-high Q-factor toroidal dipole resonance and magnetic dipole quasi-bound state in the continuum in an all-dielectric hollow metasurface. *Laser Phys.* **2022**, *32*, 025403. [[CrossRef](#)]
- Gupta, M.; Srivastava, Y.K.; Singh, R. A Toroidal Metamaterial Switch. *Adv. Mater.* **2018**, *30*, 1704845. [[CrossRef](#)]
- Butet, J.; Martin, O.J. Fano resonances in the nonlinear optical response of coupled plasmonic nanostructures. *Opt. Express* **2014**, *22*, 29693–29707. [[CrossRef](#)]
- Xiao, S.; Qin, M.; Duan, J.; Liu, T. Robust enhancement of high-harmonic generation from all-dielectric metasurfaces enabled by polarization-insensitive bound states in the continuum. *Opt. Express* **2022**, *30*, 32590–32599. [[CrossRef](#)]
- Huang, L.; Li, H.; Yu, S.; Zhao, T. Analogue of electromagnetically induced transparency inspired by bound states in the continuum and toroidal dipolar response in all-dielectric metasurfaces. *Photonic Nanostruct.* **2022**, *51*, 101041. [[CrossRef](#)]
- Modi, K.S.; Kaur, J.; Singh, S.P.; Tiwari, U.; Sinha, R.K. Extremely high figure of merit in all-dielectric split asymmetric arc metasurface for refractive index sensing. *Opt. Commun.* **2020**, *462*, 125327. [[CrossRef](#)]
- Yang, H.; Chen, Y.; Liu, M.; Xiao, G.; Luo, Y.; Liu, H.; Li, J.; Yuan, L. High Q-Factor Hybrid Metamaterial Waveguide Multi-Fano Resonance Sensor in the Visible Wavelength Range. *Nanomaterials* **2021**, *11*, 1583. [[CrossRef](#)]
- Mohammadi, M.; Seifouri, M. Numerical investigation of photonic crystal ring resonators coupled bus waveguide as a highly sensitive platform. *Photonic Nanostruct.* **2019**, *34*, 11–18. [[CrossRef](#)]
- Zhou, Y.; Guo, Z.; Zhou, W.; Li, S.; Liu, Z.; Zhao, X.; Wu, X. High-Q guided mode resonance sensors based on shallow sub-wavelength grating structures. *Nanotechnology* **2020**, *31*, 325501. [[CrossRef](#)] [[PubMed](#)]
- Li, H.; Hu, C.; Jiang, J.H.; Wu, J.; Wen, W.; Hou, B. Photonic Type-III Nodal Loop and Topological Phase Transitions at Bilayer Metasurfaces. *Front. Mater.* **2022**, *9*, 909381. [[CrossRef](#)]
- Archetti, A.; Lin, R.J.; Restori, N.; Kiani, F.; Tsoulos, T.V.; Tagliabue, G. Thermally reconfigurable metalens. *Nanophotonics* **2022**, *11*, 3969–3980. [[CrossRef](#)] [[PubMed](#)]
- Fong, K.Y.; Pernice, W.H.; Tang, H.X. Frequency and phase noise of ultra-high Q silicon nitride nanomechanical resonators. *Phys. Rev. B* **2012**, *85*, 4506. [[CrossRef](#)]
- Ji, X.; Roberts, S.; Corato-Zanarella, M.; Lipson, M. Methods to achieve ultra-high quality factor silicon nitride resonators. *APL Photonics* **2021**, *6*, 071101. [[CrossRef](#)]
- YiYang, Y.; Liu, Y.; Yang, S.; Wu, Y.; Tian, H. Double-layered silicon-nitride photonic crystal slab guided-mode-resonance high-sensitivity sensor application for refractive index sensing and nanoparticle detection. *J. Opt. Soc. Am. B* **2021**, *38*, 1927–1933. [[CrossRef](#)]
- Guo, L.; Zhang, Z.; Xie, Q.; Li, W.; Xia, F.; Wang, M.; Feng, H.; You, C.; Yun, M. Toroidal dipole bound states in the continuum in all-dielectric metasurface for high-performance refractive index and temperature sensing. *Appl. Surf. Sci.* **2023**, *615*, 156408. [[CrossRef](#)]

19. Zhou, X.; Venkatachalam, S.; Zhou, R.; Xu, H.; Pokharel, A.; Fefferman, A.; Zaknourne, M.; Collin, E. High-Q silicon nitride drum resonators strongly coupled to gates. *Nano Lett.* **2021**, *21*, 5738–5744. [[CrossRef](#)]
20. Frankis, H.C.; Kiani, K.M.; Su, D.; Mateman, R.; Leinse, A.; Bradley, J.D. High-Q tellurium-oxide-coated silicon nitride microring resonators. *Opt Lett.* **2019**, *44*, 118–121. [[CrossRef](#)]
21. Spencer, D.T.; Bauters, J.F.; Heck, M.J.; Bowers, J.E. Integrated waveguide coupled Si₃N₄ resonators in the ultrahigh-Q regime. *Optica* **2014**, *1*, 153–157. [[CrossRef](#)]
22. Ji, X.; Jang, J.K.; Dave, U.D.; Corato-Zanarella, M.; Joshi, C.; Gaeta, A.L.; Lipson, M. Exploiting Ultralow Loss Multimode Waveguides for Broadband Frequency Combs. *Laser Photonics Rev.* **2020**, *15*, 2000353. [[CrossRef](#)]
23. Domenegueti, R.R.; Zhao, Y.; Ji, X.; Martinelli, M.; Lipson, M.; Gaeta, A.L.; Nussenzeig, P. Parametric sideband generation in CMOS-compatible oscillators from visible to telecom wavelengths. *Optica* **2021**, *8*, 316–322. [[CrossRef](#)]
24. Jin, W.; Yang, Q.F.; Chang, L.; Shen, B.; Wang, H.; Leal, M.A.; Wu, L.; Gao, M.; Feshali, A.; Paniccia, M.; et al. Hertz-linewidth semiconductor lasers using CMOS-ready ultra-high-Q microresonators. *Nat. Photonics* **2021**, *15*, 346–353. [[CrossRef](#)]
25. Yu, F.; Chen, J.; Huang, L.; Zhao, Z.; Wang, J.; Jin, R.; Chen, J.; Wang, J.; Miroshnichenko, A.E.; Li, T.; et al. Photonic slide rule with metasurfaces. *Light Sci. Appl.* **2022**, *11*, 77. [[CrossRef](#)]
26. Ye, Y.; Yu, S.; Li, H.; Gao, Z.; Yang, L.; Zhao, T. Triple Fano resonances metasurface and its extension for multi-channel ultra-narrow band absorber. *Results Phys.* **2022**, *42*, 106025. [[CrossRef](#)]
27. Varasteanu, P.; Radoi, A.; Tutunaru, O.; Fica, A.; Pascu, R.; Kusko, M.; Mihalache, I. Plasmon-Enhanced Photoresponse of Self-Powered Si Nanoholes Photodetector by Metal Nanowires. *Nanomaterials* **2021**, *11*, 2460. [[CrossRef](#)]
28. Wang, W.; Zheng, L.; Xiong, L.; Qi, J.; Li, B. High Q-factor multiple Fano resonances for high-sensitivity sensing in all-dielectric metamaterials. *OSA Continuum.* **2019**, *2*, 2818. [[CrossRef](#)]
29. Li, H.; Yu, S.; Yang, L.; Zhao, T. High Q-factor multi-Fano resonances in all-dielectric double square hollow metamaterials. *Opt. Laser Technol.* **2021**, *140*, 107072. [[CrossRef](#)]
30. Biasco, S.; Beere, H.E.; Ritchie, D.A.; Li, L.; Davies, A.G.; Linfield, E.H.; Vitiello, M.S. Frequency-tunable continuous-wave random lasers at terahertz frequencies. *Light Sci. Appl.* **2019**, *8*, 43. [[CrossRef](#)]
31. Yang, L.; Yu, S.; Li, H.; Zhao, T. Multiple Fano resonances excitation on all-dielectric nanohole arrays metasurfaces. *Opt. Express* **2021**, *29*, 14905–14916. [[CrossRef](#)]
32. Fan, K.; Shadrivov, I.V.; Padilla, W.J. Dynamic bound states in the continuum. *Optica* **2019**, *6*, 169–173. [[CrossRef](#)]
33. Chen, X.; Fan, W. Tunable Bound States in the Continuum in All-Dielectric Terahertz Metasurfaces. *Nanomaterials* **2020**, *10*, 623. [[CrossRef](#)]
34. Mao, L.; Cheng, P.; Liu, K.; Lian, M.; Cao, T. Sieving nanometer enantiomers using bound states in the continuum from the metasurface. *Nanoscale Adv.* **2022**, *4*, 1617–1625. [[CrossRef](#)]
35. Cerjan, A.; Jörg, C.; Vaidya, S.; Augustine, S.; Benalcazar, W.A.; Hsu, C.W.; von Freymann, G.; Rechtsman, M.C. Observation of bound states in the continuum embedded in symmetry bandgaps. *Sci. Adv.* **2021**, *7*, eabk1117. [[CrossRef](#)]
36. Sadrieva, Z.; Frizyuk, K.; Petrov, M.; Kivshar, Y.; Bogdanov, A. Multipolar origin of bound states in the continuum. *Phys. Rev. B* **2019**, *100*, 115303. [[CrossRef](#)]
37. Koshelev, K.; Lepeshov, S.; Liu, M.; Bogdanov, A.; Kivshar, Y. Asymmetric Metasurfaces with High-Q Resonances Governed by Bound States in the Continuum. *Phys. Rev. Lett.* **2018**, *121*, 193903. [[CrossRef](#)]
38. Mi, Q.; Sang, T.; Pei, Y.; Yang, C.; Li, S.; Wang, Y.; Ma, B. High-quality-factor dual-band Fano resonances induced by dual bound states in the continuum using a planar nanohole slab. *Nanoscale Res. Lett.* **2021**, *16*, 150. [[CrossRef](#)]
39. Leitis, A.; Tittl, A.; Liu, M.; Lee, B.H.; Gu, M.B.; Kivshar, Y.S.; Altug, H. Angle-multiplexed all-dielectric metasurfaces for broadband molecular fingerprint retrieval. *Sci. Adv.* **2019**, *5*, eaaw2817. [[CrossRef](#)]
40. Reineke Matsudo, B.; Sain, B.; Carletti, L.; Zhang, X.; Gao, W.; de Angelis, C.; Huang, L.; Zentgraf, T. Efficient Frequency Conversion with Geometric Phase Control in Optical Metasurfaces. *Adv. Sci.* **2022**, *9*, e2104508. [[CrossRef](#)]
41. Abbas, M.A.; Zubair, A.; Riaz, K.; Huang, W.; Teng, J.; Mehmood, M.Q.; Zubair, M. Engineering multimodal dielectric resonance of TiO₂ based nanostructures for high-performance refractive index sensing applications. *Opt. Express* **2020**, *28*, 23509–23522. [[CrossRef](#)] [[PubMed](#)]
42. Liu, G.D.; Zhai, X.; Wang, L.L.; Lin, Q.; Xia, S.X.; Luo, X.; Zhao, C.J. A High-Performance Refractive Index Sensor Based on Fano Resonance in Si Split-Ring Metasurface. *Plasmonics* **2018**, *13*, 15–19. [[CrossRef](#)]
43. Qin, M.; Pan, C.; Chen, Y.; Ma, Q.; Liu, S.; Wu, E.; Wu, B. Electromagnetically Induced Transparency in All-Dielectric U-Shaped Silicon Metamaterials. *Appl. Sci.* **2018**, *8*, 1799. [[CrossRef](#)]
44. Zhang, Q.; Wen, X.; Li, G.; Ruan, Q.; Wang, J.; Xiong, Q. Multiple magnetic mode-based Fano resonance in split-ring resonator/disk nanocavities. *ACS Nano* **2013**, *7*, 11071–11078. [[CrossRef](#)]
45. Romano, S.; Zito, G.; Torino, S.; Calafiore, G.; Penzo, E.; Coppola, G.; Cabrini, S.; Rendina, I.; Mocella, V. Label-free sensing of ultralow-weight molecules with all-dielectric metasurfaces supporting bound states in the continuum. *Photonics Res.* **2018**, *6*, 726–733. [[CrossRef](#)]

Disclaimer/Publisher’s Note: The statements, opinions and data contained in all publications are solely those of the individual author(s) and contributor(s) and not of MDPI and/or the editor(s). MDPI and/or the editor(s) disclaim responsibility for any injury to people or property resulting from any ideas, methods, instructions or products referred to in the content.